

# The Luminous Convolution Model

S. Cisneros<sup>1</sup>, N. S. Oblath, J. A. Formaggio<sup>1</sup>, G. Goedecke<sup>2</sup>, D. Chester<sup>1,3</sup>, R. Ott<sup>1,4</sup>,  
A. Ashley<sup>1</sup>, and A. Rodriguez<sup>1</sup>

## ABSTRACT

We present a heuristic model for predicting the rotation curves of spiral galaxies. The Luminous Convolution Model (LCM) utilizes Lorentz-type transformations of very small changes in photon frequencies from curved space-times to construct a model predictive of galaxy rotation profile observations. These frequency changes are derived from the Schwarzschild red-shift result or the analogous result from a Kerr wave equation. The LCM maps the small curvatures of the emitter galactic frame onto those of the receiver galactic frame, and then returns the map to the associated flat frames where measurements are made. This treatment rests upon estimates of the luminous matter in both the emitter and receiver galaxies to determine these small curvatures. The LCM is tested on a sample of 23 galaxies, represented in 35 different data sets. LCM fits are compared to those of the Navarro, Frenk and White (NFW) Dark Matter Model, and/or to the Modified Newtonian Dynamics (MOND) model when possible. The high degree of sensitivity of the LCM to the initial assumption of a luminous mass-to-light ratio ( $M_L/L$ ) is shown. We demonstrate that the LCM is successful across a wide range of spiral galaxies for predicting the observed rotation curves.

*Subject headings:* cosmology: dark matter, theory; galaxies: distances and redshifts

## 1. Introduction

Since the 1960's, much work has been done to identify the source of what is sometimes known as the flat-rotation curve problem; that is, the discrepancy between the luminous and dynamical models of matter distributions within observed galaxies. Investigations into this problem have mainly followed one of two paths: either an alteration of the laws of physics governing gravitation or a new source of matter. The most popular among the new physics models is the Modified Newtonian Dynamics (MOF<sub>D</sub>) (Milgrom 1983), in which the gravitational constant changes gradually over the large distance scales of galaxies and clusters of galaxies. The concept of new

sources of matter is more commonly referred to as dark matter, with the most popular dark matter model to date proposed by Navarro, Frenk & White (NFW) (Navarro et al. 1997). Both approaches successfully explain a great variety of cosmological observations to date beyond spiral galaxies (for a full review of these two approaches, see Sanders & McGaugh (2002) and Gianfranco et al. (2005)). Indications of dark matter may have been observed in the DAMA (Bernabei et al. 2010), CoGeNT (Aalseth et al. 2013), and CDMS (Agnese et al. 2013) Experiments, although these results are in some conflict with the limits of XENON100 (Angle et al. 2008). Thus, despite their successes, it remains true that neither phenomena –deviations from General Relativity (GR) predictions nor direct detection of dark matter– has been observed in decisive terrestrial experiments. New clues and new approaches from particle physics and astrophysics are needed to understand the effect.

Luminous mass modeling for galaxies dates

<sup>1</sup>Laboratory for Nuclear Science, Massachusetts Institute of Technology, Cambridge, MA 02139, USA

<sup>2</sup>Department of Physics, New Mexico State University, Las Cruces, NM 88003, USA

<sup>3</sup>Present address: University of California at Los Angeles

<sup>4</sup>Present address: University of California at Davis

back to as early as 1912 with the advent of the Hertzsprung-Russell (HR) diagram (Smith 1995). The HR diagram allows for identification of mass associated with observed light. The photometric identification of the individual masses of stars is then extrapolated to population synthesis models which estimate the total luminous stellar mass of galaxies. Stellar masses are then added to estimated gas masses and reported as luminous mass-to-light ( $M_L/L$ ) ratios for a given galaxy, where  $M_L$  is the total luminous mass and  $L$  is the total luminosity.

As a constraint on the luminous masses, a second, dynamical (hence orthogonal) measurement of the mass distribution was introduced. However, this dynamical measure,  $v_{obs}$ , reported independently by Oort and Zwicky in the 1930s (Zwicky 1937; van den Bergh 1997), and later confirmed by Rubin & Ford (1975) and Bosma (1978), clearly demonstrated flat-rotation speeds at high radii, a strong deviation from the luminous Keplerian predictions. The mismatch between the dynamical ( $M'$ ) and luminous ( $M_L$ ) mass distributions within galaxies has become known as the flat-rotation curve problem. The result of the discrepancy was two fold; a ‘missing mass’ component, the dark matter ( $M_{DM}$ ), and an underconstrained luminous matter modeling problem (Conroy et al. 2009).

We propose a new model to rectify the differences between galactic rotation curves and luminous mass models. This predictive model, which we will refer to as the Luminous Convolution Model (LCM), provides an alternative to the dark matter and MOND hypotheses: it represents a new approach to rectifying the observed galaxy masses  $M'$  with the luminous galaxy masses  $M_L$ , and is constructed entirely from the luminous matter  $M_L$ . The LCM relies upon the GR evaluation of small galactic curvatures, mapped from an emitter galaxy onto the receiver galaxy, to compare the relative gravitational potentials. All evaluations of galaxies are done under idealized geometries and assumptions consistent with the current Newtonian treatment of the dark-matter problem. External factors such as the Hubble flow are assumed to be incorporated into the results of the two free parameters of the model. As this is a

heuristic model, physical interpretation of the two parameters will be left for future work.

The LCM borrows concepts from both models of modified gravity and dark matter to be consistent with the formalisms developed to date. Similar to MOND we will consider the concept of small changes to gravitational acceleration at large distances, though we will interpret the changes in acceleration as small changes in curvature. The changes in curvature will be evaluated by an appropriate homogeneous wave equation as gravitationally shifted frequencies. We will use the convenient parametrization of the rotation curve velocity prediction,  $v_{tot}$ , that is typically used in dark-matter models:

$$v_{tot}^2 = v_{lum}^2 + v_{DM}^2, \quad (1)$$

where  $v_{DM}$  is the model specific dark matter contribution, and  $v_{lum}$  is the Keplerian contribution to the rotations from the luminous component,  $M_L$ . The velocity prediction will be fit to the observed rotation velocities  $v_{obs}$ .

The paper is divided as follows. Section 2 briefly describes the formalism adopted in comparing the mass distributions of galaxies. Section 3 introduces the LCM formalism, and Section 4 reports the LCM results for 23 spiral galaxies, represented in 35 different data sets. Some general conclusions are presented in Section 5.

## 2. Mass Distributions in Spiral Galaxies

### 2.1. Spherical Symmetry

The quadratic velocity sum in Eq. (1) comes from the sum of the mass elements,

$$M' = M_L + M_{DM}, \quad (2)$$

where  $M'$  is the total gravitational mass, composed of the luminous  $M_L$  and dark  $M_{DM}$  masses. Each mass in Eq. (2) is the mass enclosed up to a radius  $r$ ,  $M(r)$ , and is related to an associated orbital velocity  $v(r)$  by Newton’s second law. In the case of spherical symmetry, that relation is simply:

$$F(r) = -\frac{mv(r)^2}{r} = -\frac{mM(r)G}{r^2}, \quad (3)$$

where  $m$  is the mass of a test particle orbiting at a radial distance  $r$  from the center of the spherical mass distribution  $M(r)$ ,  $G$  the gravitational constant, and  $F(r)$  the Newtonian gravitational force. Hence the resulting quadratic sum of velocities in Eq. (1) implies like geometry for the components summed.

The most commonly employed geometry is spherical, as the matter distribution is very diffuse. Deviations from spherical symmetry are higher order corrections to the potential and thereby the force (Binney & Tremaine 2008). Newtonian gravity potentials

$$\Phi(r) = -\frac{1}{m} \int F(r) dr + \Phi_o, \quad (4)$$

are related to forces  $F(r)$  in the traditional way. The integration constant  $\Phi_o$  is generally fixed such that  $\Phi(r) \rightarrow 0$  as  $r \rightarrow \infty$ . The gauge choice for a system of two galaxies will be discussed in Sect.3.6.

The gravity potential  $\Phi(r)$  used in the LCM will be evaluated for the luminous matter  $M_L$  alone, and hence will be called  $\Phi_L$ . The LCM is applied in the weak field limit of spiral galaxies, in which case the GR metric  $g_{\mu\nu}$  can be parametrized with the Newtonian potentials  $\Phi_L$ . The small curvature contributions convolved in the LCM function,  $v_{LC}^2$ , defined in Eq. (12), will come from scalar wave equations (Sect. 3.4 and 3.5). It is “the metric  $g_{\mu\nu}$  which forms the components of the gravitational potential” (see Einstein et al. 1923, p.204). Each data set reported the observed velocities in the context of comparison to the luminous mass model chosen. The stellar  $M_L/L$  ratios used for each galaxy are reported in Table.1.

## 2.2. Luminous Galaxy Mass

Estimates of the total luminous mass in spiral galaxies vary widely, as the modeling process is underconstrained. Models for the total light, interpreted for distance and extinction corrections, are done in specific wavelength bands. These associated bands and the  $M_L/L$  ratios reported in each source are reported in Table.1. These  $M_L/L$  ratios are generally chosen in the context of a specific model, which are also reported in Table.1.

Luminous masses  $M_L$  are reported as the Keplerian rotation velocities  $v_{lum}$  implied by Eq. (3). Luminous matter models involve assumptions regarding metallicities, types of stars, and geometries of the individual components of the galaxies; the thin and thick stellar disks, stellar bulge, and gas. In general, these components are modeled individually using different observational techniques (Binney & Tremaine 2008). The individual geometries used to calculate the appropriate potentials, and hence force relations, are not considered when the final velocity sum is calculated. The total Keplerian rotation velocity  $v_{lum}$  is taken to be the quadratic sum of the components (Gentile et al. in press), as was done for Eq. (1),

$$v_{lum}^2 = v_{bulge}^2 + v_{disk1}^2 + v_{disk2}^2 + v_{gas}^2. \quad (5)$$

This sum is an implicit assumption of like geometry for the components, as it arises from the mass sum,

$$M_{lum} = M_{bulge} + M_{disk1} + M_{disk2} + M_{gas}. \quad (6)$$

The error introduced in assuming like geometry (in Eqs. (1) or (5)) for disk and spherical mass distributions is an underestimate in the magnitude of the Newtonian gravitational potential  $\Phi(r)$  (Chatterjee 1987), not in the functional shape. As such, the introduction of such an error can not be responsible for the dark matter problem, which is a functional difference in the potential at large  $r$ .

The spherical assumption in Eq. (3) is commonly employed and offers the additional benefit of Newton’s shell theorem, where the gravitational field at each point  $r$  is composed of contributions from only those mass elements *interior* to  $r$  (Fowles & Cassidy 2005). The shell theorem will be advantageous in construction of the LCM, allowing use of the exterior metric in the plane of the galactic disk.

## 2.3. Doppler Shifts

The LCM will rely upon three different types of frequencies that are related to the general Lorentz Doppler shift formula.

The general Lorentz Doppler shift formula is applicable in a variety of contexts, from earth-bound measurements to cosmological distance

estimates. A general definition of the Lorentz Doppler shift formula (LDSF), Eq. 7,

$$\frac{v}{c} = \frac{\frac{\omega_s}{\omega_o} - \frac{\omega_o}{\omega_s}}{\frac{\omega_s}{\omega_o} + \frac{\omega_o}{\omega_s}}, \quad (7)$$

relates the characteristic frequency  $\omega_o$  to the received shifted frequency  $\omega_s$  for some photon. The relative velocity parameter  $v$  describes the motion of the source with respect to the receiver directly towards or away from each other. The characteristic frequency  $\omega_o$  is typically identified for some well known atomic transition, as measured on earth. This frequency is assumed to be the same in any flat frame in any system based upon the constancy of the speed of light.

In the context of astrophysics, when  $\omega_s > \omega_o$  the light is considered to be blue-shifted, and when  $\omega_s < \omega_o$ , the light is considered to be red-shifted. Cosmological distance indicators, translational effects (e.g. relative motion), and gravitational effects are all characterized by the dimensionless quantity  $z$ :

$$1 + z = \frac{\omega_o}{\omega_s}. \quad (8)$$

For red-shifts  $z$  is positive and for blue shifts  $z$  is negative (Hartle 2003).

The three frequencies of interest are based upon the two fundamental observables in the flat-rotation curve problem. The first observable is the shifted frequency  $\omega'$ , measured as a function of radius for a given galaxy. The second observable is the total light, which when interpreted through a population synthesis model gives the luminous mass  $M_L$ . This luminous mass implies the Keplerian rotation term  $v_{lum}$  in Eq. (1), by Eq. (3).

The first frequency of interest is the observed frequency  $\omega'$ . This frequency yields the observed flat-rotation curve velocity parameter  $v_{obs}$  by a LDSF,

$$\frac{v_{obs}}{c} = \frac{\frac{\omega'}{\omega_o} - \frac{\omega_o}{\omega'}}{\frac{\omega'}{\omega_o} + \frac{\omega_o}{\omega'}}. \quad (9)$$

The shifted-frequency  $\omega'$  is assumed to be measured for a photon emitted along the line of sight from a test particle in a stable, circular orbit. The characteristic frequency  $\omega_o$  remains defined as in

Eq. (7). The shifted frequency  $\omega'$  implies the total gravitational mass  $M'$  in Eq. (2) by Newton's second law, Eq. (3).

The second frequency of interest is that frequency which would have been measured if the luminous matter alone were responsible for the observed rotations. The Keplerian rotation velocity  $v_{lum}$  implies a frequency  $\omega_l$  by the LDSF relation:

$$\frac{v_{lum}}{c} = \frac{\frac{\omega_l}{\omega_o} - \frac{\omega_o}{\omega_l}}{\frac{\omega_l}{\omega_o} + \frac{\omega_o}{\omega_l}}. \quad (10)$$

The frequency  $\omega_l$  will be used to characterize our knowledge of the local frames in Sect.3.1. The characteristic frequency  $\omega_o$  remains defined as in Eq. (7).

The third type of frequency of interest are those from gravitational effects, often known as gravitational redshifts. For these gravitationally shifted frequencies, the associated curvatures of the space-time will be derived in Sect. 3.4 and 3.5 for the luminous matter  $M_L$  alone. These frequencies reflect metric curvature of the space-time and will be denoted as  $\omega_{gal}$  for the emitter-galaxy and  $\omega_{mw}$  for the receiver galaxy. These two gravitationally shifted frequencies will be convolved by an application of the LDSF as a mapping in Sect. 3.1.

### 3. The Luminous Convolution Model

Constructed in analogy to Eq. (1), the LCM rotation curve prediction  $v_{Lmod}$  is:

$$v_{Lmod}^2 = \zeta v_{lum}^2 + \alpha v_{LC}^2, \quad (11)$$

where  $\zeta$  and  $\alpha$  are the fitting parameters of the model,  $v_{lum}^2$  is the square of the Keplerian rotation velocity, and  $v_{LC}^2$  is the convolution term, to be defined in Sect.3.1. We will fit  $v_{Lmod}$  to the observed rotation curve data  $v_{obs}$ . The parameter  $\zeta$  scales the luminous mass distribution. The parameter  $\alpha$  relates the LCM function  $v_{LC}^2$  to the dark matter term  $v_{DM}^2$  in Sect.3.2. The  $v_{LC}^2$  requires two inputs: the luminous matter  $M_L$  profiles of both the emitter and the receiver galaxies.

The parametrization in Eq. (11) is convenient, as it allows the LCM to isolate effects on the

photons from translation and acceleration. As is known to occur in nature, effects on electric and magnetic fields (hence light) separate cleanly into two separate terms based upon the translation and acceleration of the source of the fields (see Jackson 1999, Eqs. (14.13) & (14.14)). Translation effects will be encapsulated in the term  $v_{lum}^2$  and curvature (e.g. acceleration) effects will be encapsulated in the term  $v_{LC}^2$ . As we transition from Newtonian to General Relativity, we readily replace the word acceleration with curvature.

### 3.1. Convolution Term $v_{LC}^2$

The convolution term  $v_{LC}^2$  in Eq. (1) is composed of three terms:

$$v_{LC}^2 = \kappa v_1 v_2, \quad (12)$$

where  $\kappa$  is the ratio of galactic curvatures,  $v_1$  is a mapping of the galactic frames, and  $v_2$  is a mapping back to the associated flat tangent frames where physical measurements are made.

The first term in Eq. (12),  $\kappa$ , is a measure of the deviation from flat space-time for a given pair of emitter-receiver galaxies:

$$\kappa = \frac{\Delta c_{gal}}{\Delta c_{mw}}, \quad (13)$$

where curvatures are measured based upon the difference of the coordinate light speed  $\tilde{c}_i$  from  $c$  (see Sect. 3.3),

$$\Delta c_i = c - \tilde{c}_i \quad (14)$$

for the emitter-galaxy  $i = gal$  and the receiver galaxy  $i = mw$ . The quantity  $\Delta c_i$  is sensitive to small curvatures. Physically,  $\kappa = 1$  when the two galaxies have equal deviations from flatness (i.e. the luminous galaxy masses are approximately the same as a function of radius);  $\kappa < 1$  when the emitter-galaxy is less massive than the MW, and vice versa for  $\kappa > 1$ . The  $\kappa$  ratio acts to normalize the two galactic frames to the same ‘level,’ so we can apply LDSF in a series of two mappings. As  $\kappa$  is undefined in the limit  $\Delta c_i \rightarrow 0$ , the LCM is only applicable in circumstances for which both emitter and receiver frames have non-zero curvature. However, as the curvatures for spiral galaxies are exceedingly small, this constraint does not exclude

work in very diffuse space-times.

The second term in Eq. (12),  $v_1$ , is a mapping of the galactic frames. In order to construct this mapping, we first investigate the geometric interpretation of the LDSF. We can rewrite Eq. (7) as a hyperbolic rotation

$$\frac{v}{c} = \tanh \xi = \frac{e^\xi - e^{-\xi}}{e^\xi + e^{-\xi}}, \quad (15)$$

through the rapidity angle  $\xi$ , as shown in Fig. 1.

The angle  $\xi$  is defined as a positive rotation away from the vertical time axis within the Special Relativistic light-cone (Misner et al. 1970, p67). As Special Relativity is symmetric between the two frames (i.e. it is meaningless to assign absolute motion to either frame), this rotation angle must always be positive. However, as we transition to curved frames, it is important to consistently associate the emitted and received frequencies with specific frames. In Fig. 1, we associate the characteristic frequency  $\omega_o$  with the emitter’s frame, as seen by an observer at the point of emission, and the shifted-frequency,  $\omega_s$  with the receiver’s frame.

By comparing Eq. (7) to Eq. (15), we define what we will call a fundamental convolution of frequencies (FCF):

$$e^\xi = \frac{\omega_s}{\omega_o}. \quad (16)$$

which will be used to map frames based upon ratios of frequencies emitted and received. The use

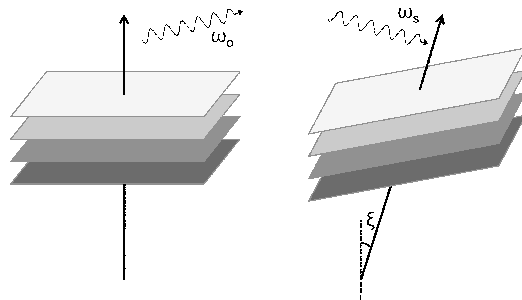


Fig. 1.— A graphic representation of a Lorentz transformation as a mapping from emitter to receiver frame. The mapping of frames will be defined by the frequencies.

of light to define the mapping of frames is apt, as light defines the metric and thereby the curvatures on any space-time.

The FCF for the  $v_1$  mapping,  $e^{\xi_1}$ , is defined by the gravitationally shifted frequencies for the emitter and receiver galaxies,  $\omega_{gal}$  and  $\omega_{mw}$ , defined in Sect. 3.4 and 3.5. The galactic FCF

$$e^{\xi_1} = \frac{\omega_{mw}}{\omega_{gal}}, \quad (17)$$

yields, by the general LDSF,

$$\frac{v_1}{c} = \frac{\frac{\omega_{mw}}{\omega_{gal}} - \frac{\omega_{gal}}{\omega_{mw}}}{\frac{\omega_{mw}}{\omega_{gal}} + \frac{\omega_{gal}}{\omega_{mw}}}. \quad (18)$$

The *parameter*  $v_1$  describes the mapping, not a physical speed. The use of the LDSF for slightly curved frames is justified by the weak field assumptions, which are in common use for evaluation of the flat-rotation curve problem.

The second term in Eq. (12),  $v_2$ , is a mapping back to the flat frames where physical measurements are made. The FCF for the  $v_2$  mapping,  $e^{\xi_2}$ , is defined by four frames: the two curved frames of the emitter/receiver galaxies  $e^{\xi_{curved}}$  and the two flat tangent frames  $e^{\xi_{flat}}$  of the emitter/receiver galaxies. This FCF is defined

$$e^{2\xi_2} = e^{\xi_{flat}} / e^{\xi_{curved}}. \quad (19)$$

where the curved FCF is  $e^{\xi_{curved}} = e^{\xi_1}$ , from Eq. (17). The FCF for the flat frames is defined by our expectation of the frequencies in Eq. (10):

$$e^{\xi_{flat}} = \left( \frac{\omega_l}{\omega_o} \right); \quad (20)$$

which describe our understanding of the luminous matter  $M_L$  within the Newtonian limit, and thereby the associated flat frames of the emitter and receiver.

In order to convolve the FCF of Eq. (19) into the  $v_2$  LDSF, we must assess the quality of a transformation from a curved to a flat frame. In Eqs. (7) and (15) boosts are always defined as positive rotations away from the time axis in Fig. 1, since the ‘rest’ frame is arbitrary. However, since it is the rest frame which we associate with the

flat frames in Eq. (20), we need to construct a reverse boost.

A reverse boost does not exist in Special Relativity, but we propose the the reciprocal of Eq. (15):

$$\frac{v_2}{c} = \coth \xi_2 = \frac{e^{\xi_2} + e^{-\xi_2}}{e^{\xi_2} - e^{-\xi_2}}, \quad (21)$$

Since the  $v_2$  is a mapping of four frames it is convenient to rewrite Eq. (21) in the form:

$$\frac{v_2}{c} = \frac{e^{2\xi_2} + 1}{e^{2\xi_2} - 1}, \quad (22)$$

such that the last mapping,  $v_2$ , is

$$\frac{v_2}{c} = \frac{\frac{\omega_l}{\omega_o} + \frac{\omega_{mw}}{\omega_{gal}}}{\frac{\omega_l}{\omega_o} - \frac{\omega_{mw}}{\omega_{gal}}}. \quad (23)$$

Again,  $v_2$  is a *parameter* describing the mapping, not a physical velocity.

### 3.2. Parameters $\zeta$ and $\alpha$

The luminous mass  $M_L$  is treated as an adjustable parameter in models such as NFW or MOND, as can be seen in Fig. 2 for eight galaxies where we have multiple data sets. The variability in the reported  $M_L$  distribution for a single galaxy is due to the underconstrained nature of luminous-matter modeling (Conroy et al. 2009; Navarro 1998). The first LCM fitting parameter  $\zeta$  allows model flexibility, as a dimensionless scaling of the luminous matter profiles given in the context of another model.

TABLE 1  
LUMINOUS MASS-TO-LIGHT RATIOS

| Galaxy     | Band <sup>a</sup> | $M_L/L^b$                                  | Model <sup>c</sup> | Reference <sup>d</sup> |
|------------|-------------------|--|--------------------|------------------------|
| NGC 3198   | B                 | 1.1  | NFW                | 2                      |
| NGC 3198   | B                 | 3.8  | NFW                | 9                      |
| NGC 3198** | $3.6\mu m$        | $1.00_{\text{bulge}}, 0.64_{\text{disk}}$  | NFW                | 4                      |
| NGC 3198   | B                 | $0.48_{\text{disk}}$                       | MOND               | 6                      |
| M 33       | $2.6mm$           | 1.0  | NFW                | 3                      |
| M 33       | $3.6\mu m$        | 1.25                                       | NFW                | 8                      |
| NGC 5055   | F                 | $3.6_{\text{disk}}$                        | NFW                | 1                      |
| NGC 5055** | $3.6\mu m$        | $1.0_{\text{disk}}$                        | NFW                | 4                      |
| NGC 5055   | $3.6\mu m$        | $0.56_{\text{bulge}}, 0.55_{\text{disk}}$  | MOND               | 5                      |
| NGC 2403   | B                 | 1.6  | MOND               | 2                      |
| NGC 2403   | $3.6\mu m$        | 0.41                                       | NFW                | 4                      |
| NGC 3521   | $3.6\mu m$        | $0.71_{\text{disk}}$                       | MOND               | 5                      |
| NGC 2841** | $3.6\mu m$        | $0.89_{\text{bulge}}, 1.26_{\text{disk}}$  | NFW                | 4                      |
| NGC 2841   | $3.6\mu m$        | $1.04_{\text{bulge}}, 0.89_{\text{disk}}$  | MOND               | 5                      |
| NGC 7814   | $3.6\mu m$        | $0.71_{\text{bulge}}, 0.68_{\text{disk}}$  | NFW                | 11                     |
| NGC 7331   | B                 | $1.8_{\text{bulge}}, 2.0_{\text{disk}}$    | MOND               | 2                      |
| NGC 7331   | $3.6\mu m$        | $1.22_{\text{bulge}}, 0.40_{\text{disk}}$  | MOND               | 5                      |
| NGC 891    | $3.6\mu m$        | $1.63_{\text{bulge}}, 0.77_{\text{disk}}$  | IND                | 11                     |
| M 31       | B                 | 2.8 – 6.5                                  | IND                | 10                     |
| NGC 5533   | B                 | 3.4  | MOND               | 7                      |
| UGC 6973   | B, R              | 2.7, 0.4                                   | MOND               | 7                      |
| NGC 4088   | B, R              | 1.0, 0.7                                   | MOND               | 13                     |
| NGC 3992   | B,R               | 4.9, 2.2                                   | MOND               | 7                      |
| NGC 4138   | B,R               | 3.5, 1.0                                   | MOND               | 13                     |
| NGC 6946   | B                 | 0.5  | MOND               | 7                      |
| NGC 6946   | $3.6\mu m$        | $1.002_{\text{bulge}}, 0.64_{\text{disk}}$ | NFW                | 4                      |
| NGC 3953   | B,R               | 2.7, 0.9                                   | MOND               | 7                      |
| NGC 2903   | B, R              | 3.6, 2.6                                   | MOND               | 7                      |
| NGC 2903** | $3.6\mu m$        | $0.61_{\text{disk}}, 1.30_{\text{bulge}}$  | NFW                | 4                      |
| NGC 2903   | $3.6\mu m$        | $1.71_{\text{disk}}$                       | MOND               | 5                      |
| NGC 5907   | B,R               | 3.9, 2.0                                   | MOND               | 13                     |
| NGC 3726   | B,R               | 1.1, 0.6                                   | MOND               | 12                     |
| F 563-1    | R                 | 6.3  | NFW                | 9                      |
| NGC 925    | $3.6\mu m$        | 0.65                                       | NFW                | 4                      |
| NGC 7793   | B                 | 2.8 – 6.5                                  | MOND               | 5                      |

NOTE.—

<sup>a</sup>Wavelength band for observations of total light.

<sup>b</sup>Reported stellar mass-to-light ratios  $M_L/L$ , in units of ( $M_\odot/L_\odot$ ).

<sup>c</sup>Model context of  $M_L$ : NFW, MOND, or IND (model independent).

<sup>d</sup>**References.** 1: Battaglia et al. (2006), 2: Bottema & Pestana (2002), 3: Corbelli (2003), 4: de Blok et al. (2008), 5: Gentile et al. (2011), 6: Gentile et al. (in press), 7: Sanders & McGaugh (2002), 8: Seigar (2011), 9: Navarro (1998), 10: Carignan & Chemin (2006), 11: Fraternali et al. (2011), 12: Sanders (1996), 13: Sanders & Verheijen (1998).

The second parameter in Eq. (11),  $\alpha$ , is presupposed to embody the relationship between the luminous convolution and dark matter

$$v_{DM}^2 = \alpha v_{LC}^2. \quad (24)$$

This parameter, unlike those of MOND or NFW, does not have a physical interpretation, but rather is a dimensionless number which characterizes the ratio of the dark matter mass to the luminous convolution term. The substitution of  $\alpha v_{LC}^2$  for  $v_{DM}^2$  in Eq. (11) does not correspond to models such as MOND, however it does add another perspective to the work on a 'universal rotation curve' by Persic et al. (1996); Persic & Salucci (1997); Rubin et al. (1980). The universal rotation curve phenomenon shows the distribution of luminous matter 'traces' the dark matter by a relationship with a median value at the luminosity of the Milky Way. Our preliminary investigation into  $\alpha$  are shown in Sect.4.2, and seem to substantiate the special status of the Milky Way's luminous mass as a critical point in the relationship between dark and luminous matter.

### 3.3. Curvature Contributions

The LCM approach arises from two assumptions. The first is that even in a curved spacetime we can always define a local Lorentz frame, which allows us to locally define the energy  $E$  of a photon (Hartle 2003) as

$$E = -\mathbf{u} \cdot \mathbf{k} = \hbar\omega_o = -(u^t k_t + \vec{k} \cdot \vec{u}), \quad (25)$$

where  $\mathbf{u}$  is the 4-velocity of the local observer,  $\mathbf{k}$  is the photon 4-momentum<sup>1</sup>,  $\vec{u}$  is the spatial 3-vector of  $\mathbf{u} = (u^t, \vec{u})$ , and  $\vec{k}$  is the wave 3-vector of  $\mathbf{k} = (k^t, \vec{k})$ .

The second aspect is that the photon can be propagated out to asymptotic infinity, enduring only negligible bending of its ray path. This argument allows us to use the eikonal approximation (Born & Wolf 1999) to solve a wave equation for the effective index of refraction. One can not always neglect deviations of light geodesics from straight lines. Therefore, in general one is forced to integrate the geodesic equations numerically,

Asaoka (1989). However, in the eikonal limit, as justified by the highly diffuse matter distribution of spiral galaxies, ray optics allows us to focus only on the magnitude of the curvature.

We assume that the scalar wave equation will capture the relevant physics in the eikonal limit. This wave equation for a photon with a wavefunction  $\Psi(x)$  is

$$\square\Psi = \frac{1}{\sqrt{g}} \frac{\partial}{\partial x^\mu} \left( g^{\mu\nu} \sqrt{g} \cdot \frac{\partial}{\partial x^\nu} \right) \Psi = 0, \quad (26)$$

where  $g^{\mu\nu}$  are the contravariant metric components, and  $(g.)$  is the determinant of the matrix of covariant components  $g_{\mu\nu}$ . In the eikonal approximation for a photon with four vector  $k_\alpha = (k_t, k_i)$ , emitted in the direction tangent to a circular orbit, instantaneously the spatial wave vector  $\vec{k} = k^i \hat{\mathbf{e}}_i$  is

$$\vec{k} = k \hat{\mathbf{e}}_\varphi \quad (27)$$

where  $\hat{\mathbf{e}}_\varphi = \frac{\mathbf{e}_\varphi}{|\mathbf{e}_\varphi|} = \frac{\mathbf{e}_\varphi}{\sqrt{g_{\varphi\varphi}}}$  is a unit vector, with  $\mathbf{e}_\varphi$  the covariant basis vector. When all metric components are independent of  $t$ , the general wavefunction at a frequency  $\omega$  can be written as  $\Psi(\mathbf{r}, t) = e^{-i\omega t} \Psi(\mathbf{r}) + c.c.$ , whereby the local eikonal wave function may be written as

$$\Psi(x) = \Psi_o \exp(-i\omega t) \exp\left(i \int_{path} d\mathbf{r} \cdot \hat{\mathbf{e}}_\varphi k\right) \quad (28)$$

where  $\Psi_o$  is an amplitude,  $d\mathbf{r} = \mathbf{e}_\varphi d\varphi$ , and,  $\omega = k_t c$  is the frequency that would be observed as emitted from  $r$ , by an asymptotic flat space observer at rest.

As discussed by Narayan et al. (1997), the effects of gravitational curvature on light can be described by an effective index of refraction  $n$ , which relates the the vacuum light speed  $c$  to the coordinate light speed  $\tilde{c}$ ,  $n = c/\tilde{c}$ . Whereas the apparent slowing of the light speed in classical electrodynamics is due to the increased path length because of interactions in the medium, for gravitational effects it reflects the increased path length due to space-time curvature.

Generalized to curved space-times by a covariant wave equation, Eq. (26), the coordinate light

<sup>1</sup> $\hbar = 1$  for the remainder of this work



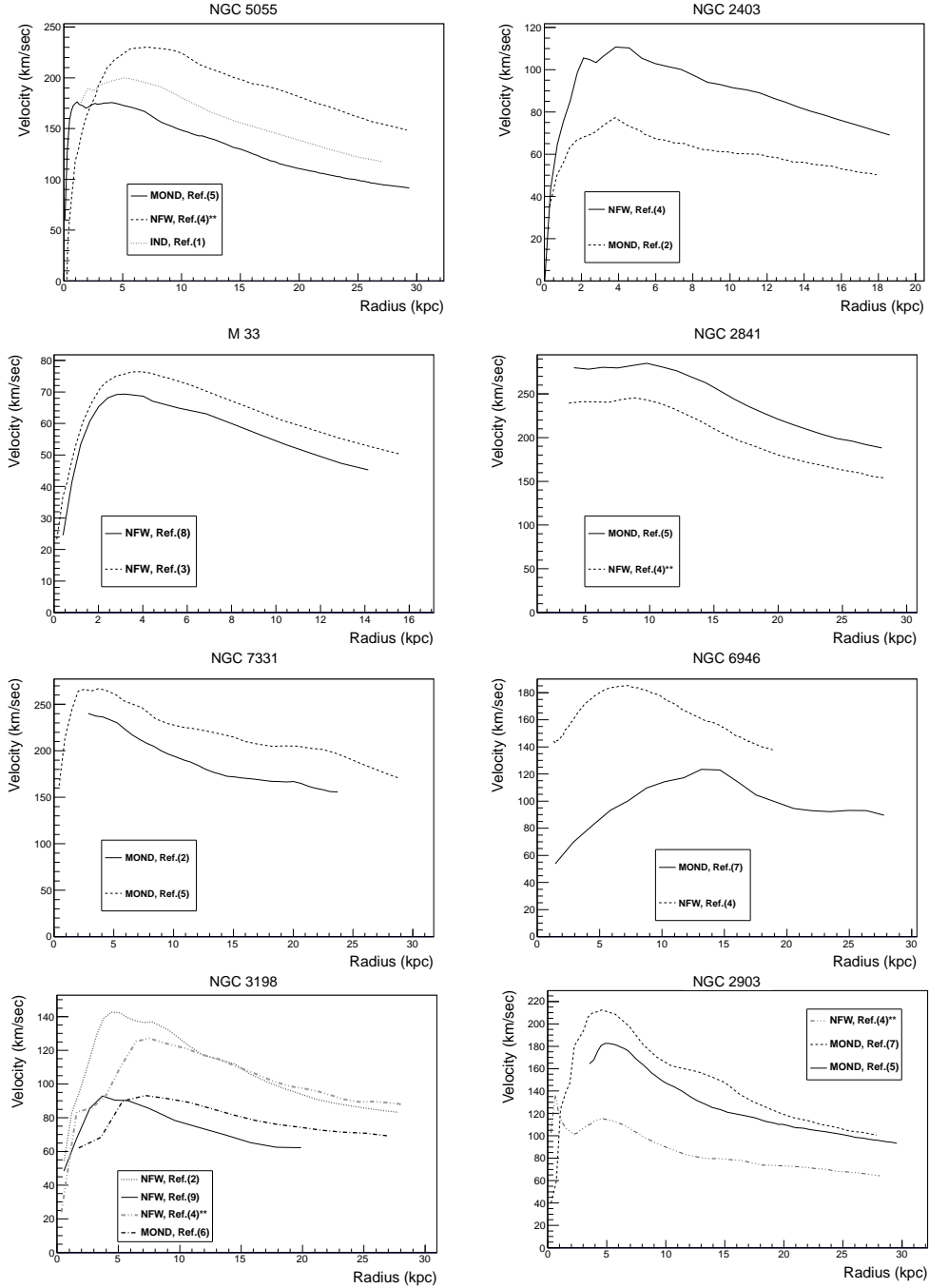


Fig. 2.— Variations in  $M_L$  reported for a different emitter galaxies.. (\*\*) after the citation indicates luminous profile which does not converge to an LCM fit. Model contexts of  $M_L$  are either NFW, MOND, or IND (model independent). References are as in Table. 1.

speed at a given radius  $r$  in a galaxy,  $\tilde{c}(r)_{gal}$ , is related to the effective index of refraction  $n(r)$  as

$$n(r) = \frac{c}{\tilde{c}(r)_{gal}}. \quad (29)$$

Wave equation solutions for Schwarzschild and Kerr are given in what follows. Both metrics used are exterior vacuum solutions, meaning they are intended for use *outside* a constant source of mass (in  $\Phi_L$ ) and  $(a)$ , the angular momentum per unit mass. Our use of these exterior metrics *inside* the plane of the galactic disc is justified by the assumption in Sect.2.2, regarding spherical symmetry and Newton's Shell theorem. This allows us to evaluate the luminous matter enclosed at each radii as the only contribution to the metric  $g_{\mu\nu}$ , by the terms  $\Phi_L$  and  $a$ , resulting in an exact solution of the Einstein equations at each radii and foliations of solutions as we move out in the radial galactic coordinate  $r$ .

The spherical assumption does break down out of the plane of the disc and close to the galactic center (due to tidal forces), or in the presence of a symmetry breaking feature such as a bar. However, in general, the inner regions of galaxies do not demonstrate the mismatch between  $M_L$  and  $M'$ , and so this assumption allows a heuristic construction of the LCM without loss of generality in regions of interest, large radii.

### 3.4. Schwarzschild Wave Equation

The Schwarzschild gravitational red-shift formula for a photon emitted at  $r$ ,

$$\frac{\omega_o}{\omega(r)} = \left( \frac{1}{\sqrt{-g_{tt}}} \right)_r, \quad (30)$$

relates the locally observed, characteristic frequency  $\omega_o$ , to the frequency received at infinity by a stationary observer  $\omega(r)$ , as a function of radial position  $r$  in the potential well. The frequency  $\omega(r)$  reflects the change in photon energy due to curvature, indicated by the Schwarzschild time metric coefficient,

$$g_{tt} = - \left( 1 - 2 \frac{GM}{c^2 r} \right) \quad (31)$$

which in the limit of weak-field metrics (Hartle 2003), is

$$g_{tt} \approx -1 + 2\Phi/c^2 \quad (32)$$

for  $\Phi$  the Newtonian gravitational potential at  $r$  the emission point, Eq. (4). All LCM calculations are made in this limit, for  $\Phi = \Phi_L$  the luminous matter Newtonian potential. Eq. (30) can be derived using either a wave equation or a Killing vector approach (Wald 1984; Cisneros et al. 2012). However, we focus on the wave equation approach, to make connection with the properties of the photon mentioned in Sect.3.

To write the Schwarzschild wave equation, consider a general Schwarzschild metric,  $(t, r, \varphi, \theta)$ , whereby the nonzero  $g_{\mu\nu}$  are  $g_{tt}, g_{\varphi\varphi}, g_{rr}$ , and  $g_{\theta\theta}$ , which are independent of  $\varphi$  and  $t$ . The components of the metric  $g$  are independent of time and have no cross terms  $g_{oi}$ , we can therefore write immediately

$$g^{00} \frac{\partial}{\partial t^2} \Psi - \frac{1}{\sqrt{g}} \frac{\partial}{\partial x^i} \left( g^{ij} \sqrt{g} \frac{\partial}{\partial x^j} \right) \Psi = 0 \quad (33)$$

where superscripts  $(ij)$  denote spatial components (Hartle 2003). For  $\theta = \pi/2$  in the plane of the disc, the Schwarzschild line element becomes

$$ds^2 = g_{tt} dt^2 + g_{rr} dr^2 + g_{\varphi\varphi} d\varphi^2. \quad (34)$$

for  $g_{rr} = 1/g_{tt}$ ,  $g_{\varphi\varphi} = r^2$ , and  $\varphi$  is the azimuthal coordinate.

In a small neighborhood of the angle  $\varphi = \varphi_o$ , for a photon emitted at  $r$ , Eq. (28) reduces to

$$\Psi(x) = \Psi_o \exp(-i\omega t) \exp(ik\sqrt{g_{\varphi\varphi}}(\varphi - \varphi_o)). \quad (35)$$

Inserting Eq. (35) into Eq. (33) yields,

$$\omega^2 [-g^{tt} - n^2 g^{\varphi\varphi} g_{\varphi\varphi}] \Psi = 0. \quad (36)$$

The general solution of Eq. (36) is

$$\frac{1}{\sqrt{-g_{tt}}} = n(r), \quad (37)$$

for  $n(r)$  the effective index of refraction, defined as Eq. (29).

In the Schwarzschild context, curvature affects only the energy (e.g. frequency) of the photon (Wald 1984),

$$n(r) = \frac{\omega_o}{\omega}, \quad (38)$$

so that Eq. (30) equals Eq. (37)

$$n(r) = \frac{c}{\tilde{c}_{gal}} = \frac{\omega_o}{\omega}. \quad (39)$$

Since it is that frequency  $\omega$  which gives information at infinity regarding the curvature at  $r$ , for some enclosed luminous mass  $M(r)_L$ , it is labeled  $\omega_{gal}$  or  $\omega_{mw}$  in what follows, to reflect said gravitational source which it describes.

Alternately, the identification of the frequencies can be demonstrated by construction of a local transformation from a Schwarzschild metric to the tangent Lorentz frame. The photon which is locally observed with an emission frequency  $\omega_o$ , is also measured by the external observer as coming from an emitter embedded in a curvature as indicated by  $\omega$ . To connect these two observations, the change of coordinates from  $(t, r, \phi) \rightarrow (\hat{t}, \hat{r}, \hat{\phi})$  is

$$\begin{aligned} dt &= \frac{d\hat{t}}{\sqrt{-g_{tt}(r)}} \\ dr &= \frac{d\hat{r}}{\sqrt{-g_{rr}(r)}} \\ rd\phi &= \hat{r}d\hat{\phi}, \end{aligned} \quad (40)$$

such that Eq. (34) becomes the local Lorentz frame

$$ds^2 = d\hat{t}^2 + d\hat{r}^2 + \hat{r}^2 d\hat{\phi}^2. \quad (41)$$

Starting at the emission point  $(r, \varphi_o)$ , the observed frequency and wavenumber  $\omega_o, k_o$  in the Lorentz frame of Eq. (41) must be related to the coordinate frequency and wavenumber  $\omega, k_r$  measured by the observer who sees the space-time as Eq. (34).

The transformation of the time dependent portion of the eikonal wave function Eq. (28), yields

$$\exp(-i\omega t) = \exp\left(-i\omega \frac{\hat{t}}{\sqrt{-g_{tt}}}\right). \quad (42)$$

The local Lorentz flat frame observer, for whom  $\omega = \omega_o$  and  $g_{tt} \rightarrow \eta_{tt} = -1$ ,

$$\exp(-i\omega t) = \exp(-i\omega_o \hat{t}) \quad (43)$$

The second observer, who sees Eq. (34), finds  $\omega = \omega_{gal}$  and  $g_{tt} = g_{tt}(r)$ , would measure

$$\exp\left(-i\omega \frac{\hat{t}}{\sqrt{-(g_{tt})_r}}\right) \equiv \exp(-i\omega_o \hat{t}). \quad (44)$$

Setting these two measurements of the same wave packet equal returns the identification of the frequencies with the gravitational red-shift

$$\omega \frac{1}{\sqrt{-(g_{tt})_r}} = \omega_o. \quad (45)$$

### 3.5. The Kerr Wave Equation

The Kerr wave equation is constructed from the covariant wave operator in Eq. (26). We consider a general Kerr-type metric in Boyer-Lindquist coordinates,  $(t, r, \varphi, \theta)$ , whereby the nonzero  $g_{\mu\nu}$  are  $g_{tt}, g_{t\varphi}, g_{\varphi\varphi}, g_{rr}$ , and  $g_{\theta\theta}$ , and are independent of  $\varphi$  and  $t$ . In Boyer-Lindquist coordinates, the exterior Kerr metric coefficients are (Chandrasekhar 1983; O'Neill 1995),

$$\begin{aligned} g_{tt} &= -(1 - 2Mr/\Sigma), \\ g_{\varphi\varphi} &= ((r^2 + a^2)^2 - a^2 \Delta \sin^2 \theta) \sin^2 \theta / \Sigma \\ g_{\theta\theta} &= \Sigma, \\ g_{rr} &= \Sigma / \Delta, \\ g_{t\varphi} &= g_{\varphi t} = -2Mar \sin^2 \theta / \Sigma \end{aligned} \quad (46)$$

where

$$\begin{aligned} \Sigma &= r^2 + a^2 \cos^2 \theta, \\ \Delta &= r^2 + a^2 - 2Mr. \end{aligned} \quad (47)$$

for  $a = J/M$  the angular momentum per unit mass, and  $M$  the enclosed mass at some radius  $r$ .

Writing the eikonal approximation, as in the previous case Eq. (35), cross terms in time and space,  $\omega k_i$ , are dropped as second order contributions. In the equatorial plane of the galaxy,  $\theta = \pi/2$ , the Kerr wave equation yields

$$\omega^2 [-g^{tt} + 2ng^{t\varphi} \sqrt{g_{\varphi\varphi}} - n^2 g^{\varphi\varphi} g_{\varphi\varphi}] \Psi = 0. \quad (48)$$

The general solution of Eq. (48) is

$$n(r) = \frac{-g_{t\varphi} \pm \sqrt{(g_{t\varphi})^2 - (g_{\varphi\varphi})(g_{tt})}}{g_{tt} \sqrt{g_{\varphi\varphi}}}. \quad (49)$$

Note that the denominator is negative, since  $g_{tt} \approx -1 + 2\Phi/c^2$  in weak-field Kerr-type metrics, where  $\Phi$  is the Newtonian gravity potential. Therefore we chose the  $(-)$  sign preceding the

square root in order to obtain a positive  $n$ .

Interpreting the effective index of refraction Eq. (49) as a ratio of frequencies to first order, as in the Schwarzschild case Eq. (39), the Kerr effective index of refraction is:

$$n(r) \approx \frac{\omega_o}{\omega_{gal}(r)}. \quad (50)$$

### 3.6. Parametrization of metric terms in the gravitational red-shifts

The construction of the LCM rotation curve prediction, Eq. (11), requires parametrizing the metric coefficients  $g_{\mu\nu}$  in either Eq. (37) or Eq. (48). The Kerr metric best mimics the physical symmetries of spiral galaxies (Hartle 2003), but the assumption in Eq. (50) is not experimentally verified. The Schwarzschild gravitational redshift result, Eq. (39), on the other hand, has been experimentally confirmed (Hartle 2003; Wald 1984). As such, the LCM function  $v_{LC}^2$  will be parametrized with Schwarzschild metric coefficients in all of the following fits. We have verified that the LCM function works equally well with either the Schwarzschild or Kerr metric, but only the Schwarzschild-metric results will be presented here.

Finally, the Schwarzschild-metric coefficient associated with time,  $g_{tt}$  in Eq. (32), is parametrized with the Newtonian gravitational potential  $\Phi_L$ , as defined in Eq. (4). The integration constant  $\Phi_o$  is generally fixed so that as  $r \rightarrow \infty$  the potential  $\Phi(r) \rightarrow 0$ .

This integration constant  $\Phi_o$  is the original gauge freedom in classical gravity. Two galaxies, with arbitrarily different luminous mass distributions will naturally have different gauges in order to meet this constraint. However, to enforce continuity and energy conservation for a photon traveling between two galaxies the two galaxy gauges,  $\Phi_{o,1}$  and  $\Phi_{o,2}$ , must be set to a common value. Consistent with Weyl's statement that, "in the physical sense, only the ratios of the  $g_{ij}$  have an immediate tangible meaning" (see Einstein et al. 1923, p.204), we arbitrarily set both gauges  $\Phi_{o,1} = \Phi_{o,2} = 0$ .

Evaluation of the Kerr metric terms requires one additional parameter: the angular momentum per unit mass,  $a$ . In the Newtonian limit,  $a$  is defined to be:

$$a(r) = \frac{J(r) = 4\pi \int_{r_1}^{r_2} \rho \Omega r^4 dr}{M(r) = r \int_{r_1}^{r_2} F(r) dr / G}, \quad (51)$$

where  $F(r)$  is the Newtonian force in Eq. (3),  $\Omega = v_{lum}/r$  is the associated angular rotation frequency, and  $\rho = M_L/(4\pi r^3/3)$  is the luminous matter density.

## 4. Validation

To validate the LCM model we perform fits of  $v_{Lmod}$  (Eq. 11) to the observed data,  $v_{obs}$ . The LCM takes the luminous mass models of both the emitter galaxy and the receiver galaxy, the Milky Way, as its inputs. For the Milky Way (MW), we use the three mass models shown in Fig. 3; though the three profiles are significantly different from one another, these differences have, in general, little impact on the LCM fit results. The emitter-galaxy data are listed in Table 1.

### 4.1. Fitting Procedure and Results

The fits between the LCM model and the  $v_{obs}$  data are calculated using the MINUIT minimization software as implemented in the ROOT data-analysis package (Brun & Rademakers 1997), with one fit being performed for every emitter/receiver galaxy pair. The fits are accomplished in two steps: The first iteration of the fit yields an initial value of  $\zeta$ , denoted  $\zeta_o$ , which is then used to rescale the luminous matter distribution  $M_L$ . The second iteration of the fit is performed using the rescaled  $M_L$  as the input luminous mass profile to calculate  $v_{Lmod}$ , resulting in the final values for  $\zeta$  and  $\alpha$ .

All of the fit results are reported in Table. 2. The fits for selected emitter/receiver galaxy pairs are shown in Figs 6, 7, and 8. Fig. 4 shows the distributions of  $\zeta_o$  and  $\zeta$  for all of the emitter/receiver galaxy pairs. For most of the galaxies the second iteration results in a better fit as well as convergence of  $\zeta_o$  to a median value of  $\zeta = 1.05 \pm 0.07$ .

In a limited number of cases (four out of 35 emitter-galaxy data sets), the fits of the reported luminous mass profiles from one particular source failed to converge. The four data sets are from de Blok et al. (2008): NGC 2903, NGC 3198, NGC 2841 and NGC 5055. The resulting parameter values are reported in Table. 2 and denoted with a double asterisk (\*\*), but these data sets are not included in the  $\alpha$  and  $\zeta$  distributions or in the subsequent fits reported in Figs.6-8. For these same galaxies, alternate luminous mass profiles are successful in LCM fits. This suggests that the LCM can potentially constrain luminous matter modeling.

#### 4.2. Results on $\alpha$

Fig. 5 shows the values of  $\alpha$  from the LCM fits as a function of the terminal value of  $\kappa$ . The terminal value of  $\kappa$ , denoted as  $\kappa_\tau$ , is the value of  $\kappa$  at the largest radius available in the data for either the emitter or the receiver galaxy, in a given galaxy pair. For the majority of emitter/receiver galaxy pairs in this analysis,  $\kappa$  approaches a constant value at large radii, as the luminous matter has been entirely enclosed.

The  $\alpha$  distribution has two interesting features. The first is that the sign of  $\alpha$  appears to be related to the astrophysical red-shift parameter,  $z$  (Eq. (8)). For values of  $\kappa_\tau < 1$ ,  $\alpha$  is negative (with the exception of NGC 925), and vice versa for  $\kappa_\tau > 1$ . Physically, emitter galaxies for which  $\kappa_\tau < 1$  are less massive than the MW; they sit in a shallower gravitational potential well. Therefore, light coming from those galaxies will be blue shifted when observed in the MW. Similarly, emitter galaxies for which  $\kappa_\tau > 1$  sit in a deeper gravitation potential well than the MW, and therefore light emitted there will be red shifted when observed in the MW. The exception to this pattern is NGC 925, for which  $\kappa$  has not yet approached a constant value at the largest extent of the data set.

The second feature of interest for the  $\alpha$  distribution is an apparent functional relationship between  $\alpha$  and the  $\kappa_\tau$ . As is shown in Fig. 5, the apparent inflection point in the distribution for the initial  $\alpha_o$  values falls slightly to the left of  $\kappa_\tau = 1$ , but after the scaling iteration, the inflection point of the

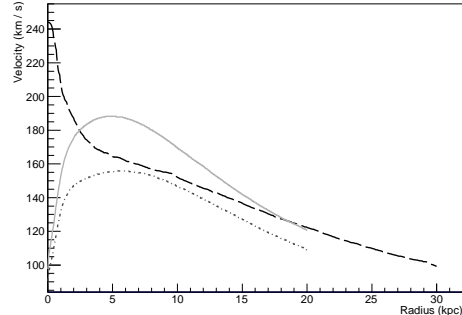


Fig. 3.— The MW luminous mass models used in this work are: Klypin et al. (2002), model A dotted-dashed line and model B solid line , Sofue & Kato (1981) dashed line.

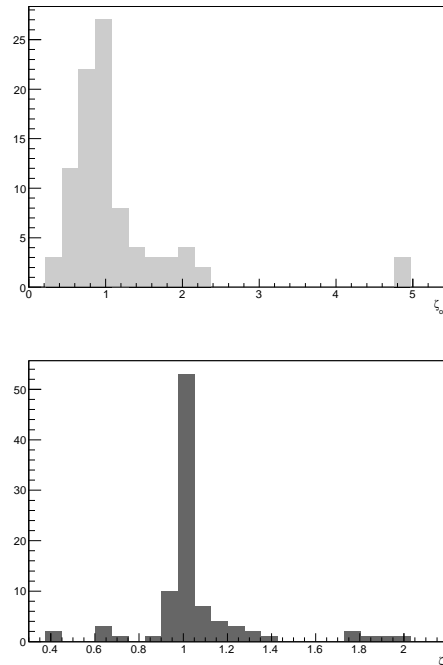


Fig. 4.—  $\zeta$  distributions: initial (top) and after scaling (bottom).

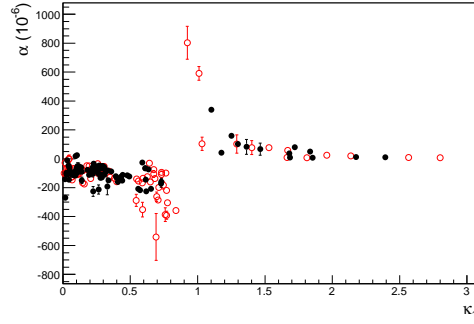


Fig. 5.— The LCM  $\alpha$  fit results vs.  $\kappa_\tau$ . Each dot represents one emitter/receiver galaxy pair) Red points represent initial  $\alpha_o$  values, and black points represent  $\alpha$  values after the scaling iteration. The error bars are only statistical uncertainties.

distribution moves to  $\kappa_\tau = 1$ . The fact that there appears to be a functional relationship between  $\alpha$  and  $\kappa_\tau$  is important because  $\alpha$  parametrizes the hypothesized relationship between the dark and luminous matter, Eq.(24).

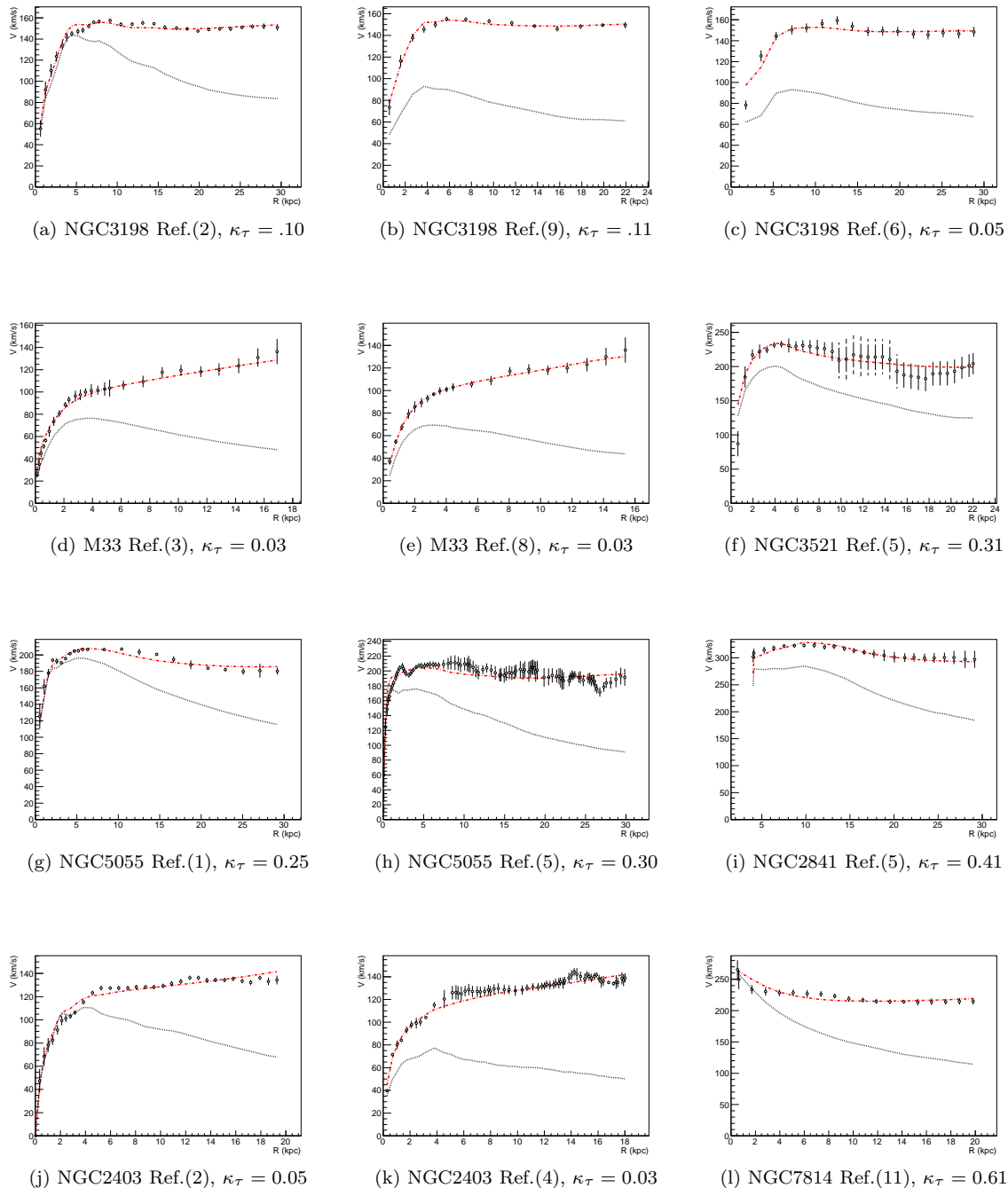


Fig. 6.— LCM fits to rotation curves of spiral galaxies with published data. Emitter-galaxies are paired to MW Sofue & Kato (1981). In all panels the black circles represent the observed rotation velocities and the thin bars represent the reported uncertainties. The dotted curve shows the Newtonian rotation curve of the luminous contributions. The LCM best-fit is shown as a red dotted-dashed line. References are as in Table 1.

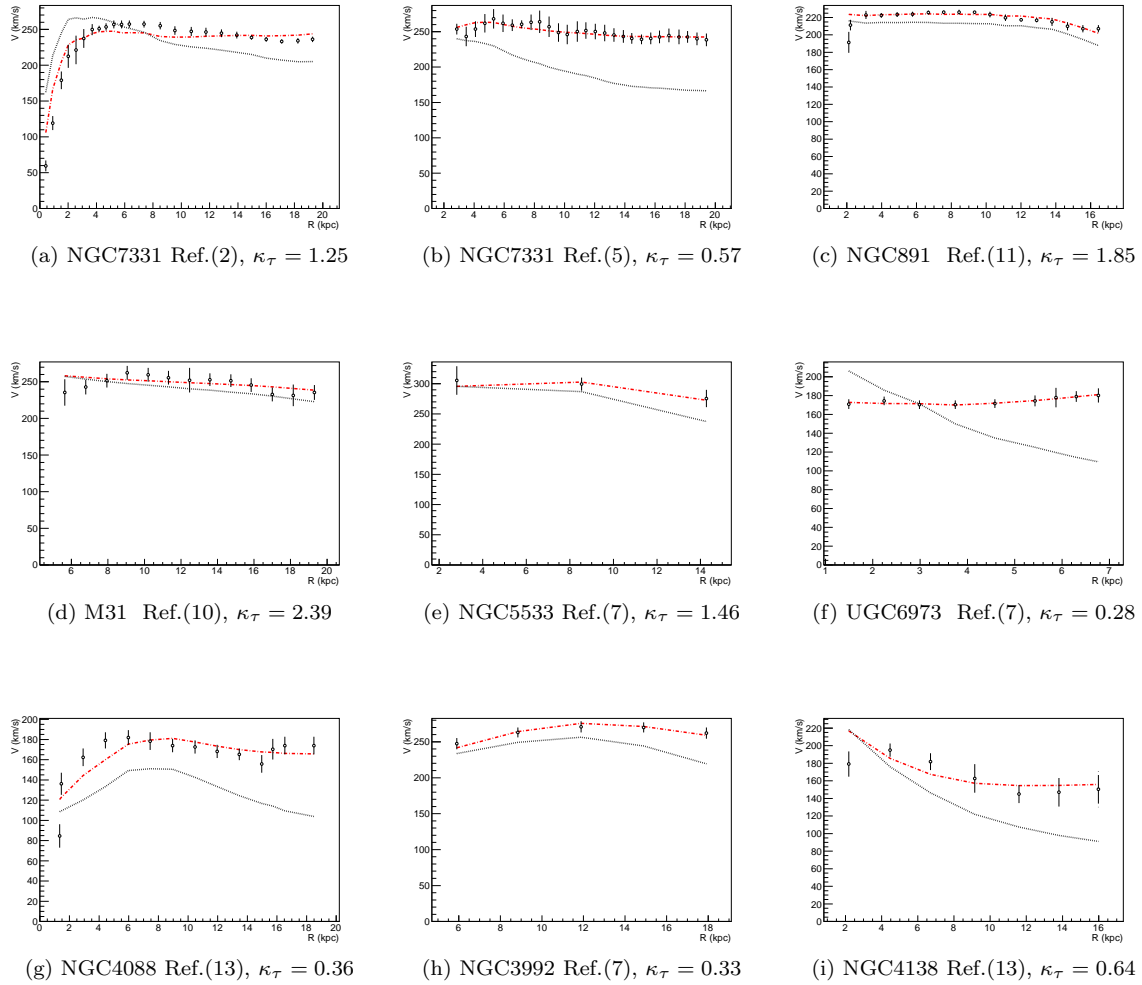


Fig. 7.— LCM fits to rotation curves of spiral galaxies with published data. Emitter-galaxies paired to MW Klypin et al. (2002, Model A). Symbols and curves are as in Figure 6, and references are as in Table.1.



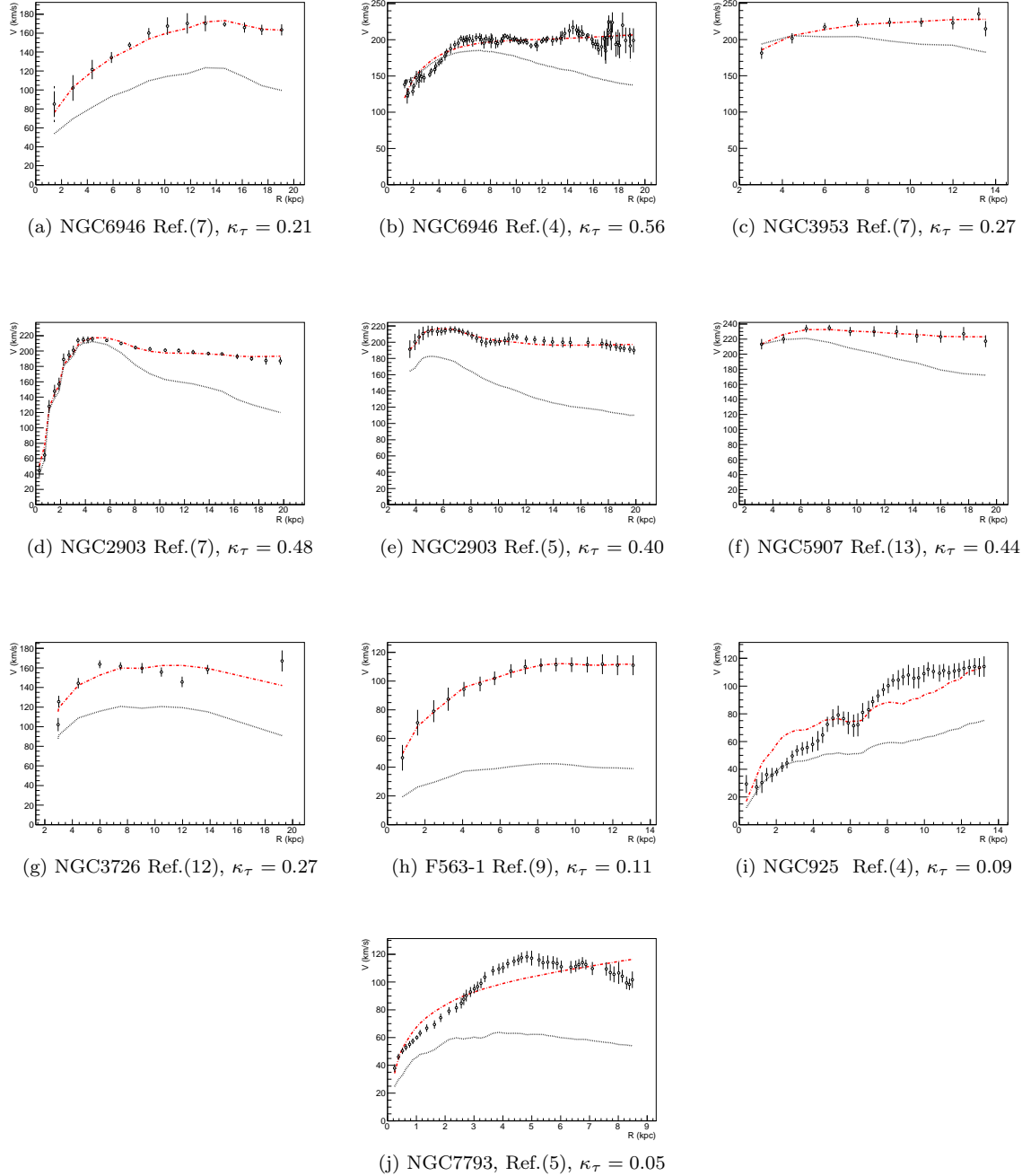


Fig. 8.— LCM fits to rotation curves of spiral galaxies with published data. Emitter-galaxies paired to MW Klypin et al. (2002, Model B). Symbols and curves are as in Figure 6, and references are as in Table.1.

TABLE 2  
RESULTS FROM LCM FITS

| Galaxy <sup>a</sup> | $\kappa_\tau$ | $\alpha^b (10^{-6})$ | $\zeta^c$       | $\zeta_o$  | LCM Fit $\frac{\chi^2}{\text{dof}}$ | Other Model $\frac{\chi^2}{\text{dof}}^d$ | Reference <sup>e</sup> | Reference <sup>f</sup> |
|---------------------|---------------|----------------------|-----------------|------------|-------------------------------------|---|------------------------|------------------------|
| NGC3198             | 0.10          | $-59.70 \pm 0.93$    | $1.00 \pm 0.01$ | 0.90       | 47.48/26 = 1.83                     | 1.34 <sub>N</sub>                         | 2                      | 16                     |
|                     | 0.26          | $-79.04 \pm 1.84$    | $1.01 \pm 0.01$ | 0.84       | 42.30/19 = 2.23                     |   |                        | 14                     |
|                     | 0.24          | $-76.28 \pm 1.77$    | $1.01 \pm 0.01$ | 0.85       | 41.99/19 = 2.21                     |   |                        | 15                     |
| NGC3198             | 0.11          | $-0.54 \pm 1.69$     | $0.99 \pm 0.01$ | 2.12       | 10.32/12 = 0.86                     | 0.67 <sub>N</sub>                         | 9                      | 16                     |
|                     | 0.31          | $-70.64 \pm 2.33$    | $0.97 \pm 0.01$ | 2.09       | 10.81/11 = 0.98                     |   |                        | 14                     |
|                     | 0.28          | $-67.61 \pm 2.23$    | $0.98 \pm 0.01$ | 2.10       | 10.76/11 = 0.98                     |   |                        | 15                     |
| NGC3198**           | 0.06          | $106.01 \pm 2.76$    | $1.02 \pm 0.02$ | 0.65       | 451.04/24 = 18.79                   | 0.84 <sub>N</sub>                         | 4                      | 16                     |
|                     | 0.09          | $-180.89 \pm 8.30$   | $1.02 \pm 0.05$ | 0.43       | 420.93/14 = 30.07                   |   |                        | 14                     |
|                     | 0.09          | $-179.37 \pm 8.21$   | $1.03 \pm 0.05$ | 0.43       | 417.12/14 = 29.79                   |   |                        | 15                     |
| NGC3198             | 0.05          | $-58.55 \pm 4.20$    | $0.99 \pm 0.02$ | 0.99       | 29.81/14 = 2.13                     | 4.48 <sub>M</sub>                         | 6                      | 16                     |
|                     | 0.23          | $-89.43 \pm 9.18$    | $0.97 \pm 0.04$ | 1.87       | 25.18/9 = 2.80                      |   |                        | 14                     |
|                     | 0.21          | $-86.58 \pm 8.89$    | $0.97 \pm 0.04$ | 1.88       | 25.31/9 = 2.81                      |   |                        | 15                     |
| M33                 | 0.03          | $-97.91 \pm 5.67$    | $1.01 \pm 0.05$ | 0.68       | 25.86/24 = 1.08                     | 0.29 <sub>N</sub>                         | 3                      | 16                     |
|                     | 0.07          | $-101.94 \pm 5.93$   | $1.02 \pm 0.05$ | 0.66       | 30.19/24 = 1.26                     |   |                        | 14                     |
|                     | 0.07          | $-100.56 \pm 5.85$   | $1.01 \pm 0.05$ | 0.67       | 29.81/24 = 1.24                     |   |                        | 15                     |
| M33                 | 0.03          | $-106.00 \pm 5.22$   | $1.00 \pm 0.04$ | 0.91       | 4.03/18 = 0.22                      | 0.16 <sub>N</sub>                         | 8                      | 16                     |
|                     | 0.07          | $-111.40 \pm 5.50$   | $1.06 \pm 0.04$ | 0.89       | 3.67/18 = 0.20                      |   |                        | 14                     |
|                     | 0.07          | $-110.00 \pm 5.45$   | $1.00 \pm 0.04$ | 0.90       | 3.65/18 = 0.20                      |   |                        | 15                     |
| NGC5055             | 0.25          | $-52.97 \pm 1.48$    | $1.01 \pm 0.01$ | 0.87       | 70.24/21 = 3.34                     | 3.96 <sub>N</sub>                         | 1                      | 16                     |
|                     | 0.31          | $-109.96 \pm 4.54$   | $2.03 \pm 0.01$ | 0.40       | 30.23/16 = 1.89                     |   |                        | 14                     |
|                     | 0.44          | $-111.50 \pm 4.60$   | $1.26 \pm 0.04$ | 0.62       | 28.93/21 = 1.81                     |   |                        | 15                     |
| NGC5055**           | 0.30          | $-39.78 \pm 3.47$    | $1.01 \pm 0.01$ | 0.86       | 4915.35/51 = 96.38                  | 75.78 <sub>N</sub>                        | 4                      | 16                     |
|                     | NA            | NA                   | NA              | $10^{-11}$ | NA                                  |   |                        | 14                     |
|                     | NA            | NA                   | NA              | $10^{-10}$ | NA                                  |   |                        | 15                     |
| NGC5055             | 0.30          | $-53.46 \pm 1.12$    | $1.00 \pm 0.01$ | 0.97       | 171.09/92 = 1.86                    | 1.05 <sub>M</sub>                         | 5                      | 16                     |
|                     | 0.39          | $-120.16 \pm 4.13$   | $1.80 \pm 0.02$ | 0.47       | 80.01/63 = 1.27                     |   |                        | 14                     |
|                     | 0.61          | $-144.63 \pm 5.04$   | $1.06 \pm 0.01$ | 0.80       | 97.42/63 = 1.55                     |   |                        | 15                     |
| NGC2403             | 0.05          | $-79.90 \pm 1.35$    | $1.01 \pm 0.01$ | 0.66       | 97.63/31 = 3.15                     | 4.98 <sub>M</sub>                         | 2                      | 16                     |
|                     | 0.14          | $-88.93 \pm 1.50$    | $1.03 \pm 0.02$ | 0.63       | 102.97/31 = 3.32                    |   |                        | 14                     |
|                     | 0.13          | $-86.90 \pm 1.47$    | $1.02 \pm 0.02$ | 0.65       | 102.53/31 = 3.31                    |   |                        | 15                     |
| NGC2403             | 0.03          | $-108.00 \pm 1.41$   | $1.00 \pm 0.02$ | 0.89       | 115.71/61 = 1.90                    | 1.81 <sub>N</sub>                         | 4                      | 16                     |

TABLE 2—*Continued*

| Galaxy <sup>a</sup> | $\kappa_\tau$ | $\alpha^b$ ( $10^{-6}$ ) | $\zeta^c$       | $\zeta_o$ | LCM Fit $\frac{\chi^2}{\text{dof}}$ | Other Model $\frac{\chi^2}{\text{dof}}^d$ | Reference <sup>e</sup> | Reference <sup>f</sup> |
|---------------------|---------------|--------------------------|-----------------|-----------|-------------------------------------|---|------------------------|------------------------|
|                     | 0.09          | $-116.41 \pm 1.52$       | $1.01 \pm 0.02$ | 0.85      | 117.99/61 = 1.93                    |   |                        | 14                     |
|                     | 0.09          | $-114.42 \pm 1.49$       | $1.01 \pm 0.02$ | 0.87      | 118.19/61 = 1.94                    |   |                        | 15                     |
| NGC 3521            | 0.31          | $-56.82 \pm 6.52$        | $0.99 \pm 0.02$ | 1.14      | 21.27/32 = 0.66                     | 0.97 <sub>M</sub>                         | 5                      | 16                     |
|                     | 0.73          | $-171.00 \pm 25.53$      | $1.02 \pm 0.03$ | 0.98      | 23.76/28 = 0.85                     |   |                        | 14                     |
|                     | 0.73          | $-158.62 \pm 23.77$      | $0.98 \pm 0.03$ | 1.07      | 24.36/28 = 0.87                     |   |                        | 15                     |
| NGC2841**           | 0.45          | $-175.00 \pm 7.57$       | $0.96 \pm 0.01$ | 1.28      | 3.61/24 = 0.15                      | 0.57 <sub>N</sub>                         | 4                      | 16                     |
|                     | 2.97          | $25.31 \pm 1.70$         | $0.48 \pm 0.01$ | 3.22      | 6.44/14 = 0.46                      |   |                        | 14                     |
|                     | NA            | NA                       | NA              | $10^{-7}$ | NA                                  |   |                        | 15                     |
| NGC2841             | 0.41          | $-160.26 \pm 8.28$       | $1.00 \pm 0.01$ | 1.02      | 20.48/22 = 0.93                     | 1.08 <sub>M</sub>                         | 5                      | 16                     |
|                     | 1.72          | $79.99 \pm 6.27$         | $0.73 \pm 0.01$ | 1.70      | 5.95/12 = 0.50                      |   |                        | 14                     |
|                     | 1.84          | $52.17 \pm 5.44$         | $0.63 \pm 0.00$ | 1.99      | 9.53/12 = 0.79                      |   |                        | 15                     |
| NGC7814             | 0.61          | $-65.63 \pm 2.03$        | $1.06 \pm 0.02$ | 0.80      | 19.38/17 = 1.14                     | 9.11 <sub>N</sub>                         | 11                     | 16                     |
|                     | 1.68          | $37.37 \pm 1.12$         | $0.96 \pm 0.03$ | 0.79      | 11.61/17 = 0.68                     |   |                        | 14                     |
|                     | 1.30          | $102.45 \pm 2.99$        | $0.61 \pm 0.04$ | 0.66      | 30.52/17 = 1.80                     |   |                        | 15                     |
| NGC7331             | 0.32          | $-88.92 \pm 2.26$        | $1.22 \pm 0.02$ | 0.51      | 270.21/32 = 8.44                    | 6.80 <sub>M</sub>                         | 2                      | 16                     |
|                     | 1.25          | $158.33 \pm 6.73$        | $1.11 \pm 0.01$ | 0.75      | 122.78/22 = 5.58                    |   |                        | 14                     |
|                     | 1.10          | $339.91 \pm 11.10$       | $1.28 \pm 0.01$ | 0.72      | 58.58/22 = 2.66                     |   |                        | 15                     |
| NGC7331             | 0.29          | $-110.00 \pm 5.47$       | $1.00 \pm 0.02$ | 1.02      | 12.01/34 = 0.35                     | 0.45 <sub>M</sub>                         | 5                      | 16                     |
|                     | 0.57          | $-217.52 \pm 15.53$      | $1.29 \pm 0.03$ | 0.74      | 5.821/26 = 0.22                     |   |                        | 14                     |
|                     | 0.62          | $-225.56 \pm 16.11$      | $1.08 \pm 0.03$ | 0.88      | 5.91/26 = 0.23                      |   |                        | 15                     |
| NGC891              | 0.59          | $-25.22 \pm 11.24$       | $1.02 \pm 0.04$ | 0.92      | 27.74/16 = 1.73                     | IND                                       | 11                     | 16                     |
|                     | 1.85          | $6.54 \pm 3.11$          | $1.00 \pm 0.02$ | 1.02      | 28.42/16 = 1.78                     |   |                        | 14                     |
|                     | 1.69          | $8.66 \pm 4.92$          | $1.00 \pm 0.02$ | 1.01      | 29.74/16 = 1.86                     |   |                        | 15                     |
| M 31                | 1.18          | $42.14 \pm 19.02$        | $0.88 \pm 0.02$ | 1.14      | 7.93/21 = 0.38                      | IND                                       | 10                     | 16                     |
|                     | 2.39          | $10.19 \pm 6.76$         | $1.00 \pm 0.08$ | 0.85      | 8.05/11 = 0.73                      |   |                        | 14                     |
|                     | 2.18          | $12.30 \pm 8.83$         | $1.00 \pm 0.09$ | 0.85      | 8.381/11 = 0.76                     |   |                        | 15                     |
| NGC 5533            | 0.43          | $-124.00 \pm 18.01$      | $1.04 \pm 0.06$ | 0.79      | 1.35/3 = 0.45                       | 3.55 <sub>M</sub>                         | 7                      | 16                     |
|                     | 1.46          | $67.00 \pm 41.61$        | $0.99 \pm 0.04$ | 1.04      | 0.29/1 = 0.29                       |   |                        | 14                     |
|                     | 1.36          | $82.83 \pm 51.61$        | $0.99 \pm 0.04$ | 1.06      | 0.31/1 = 0.31                       |   |                        | 15                     |
| UGC 6973            | 0.10          | $-99.10 \pm 5.35$        | $1.02 \pm 0.03$ | 0.54      | 0.60/7 = 0.09                       | 23.50 <sub>M</sub>                        | 7                      | 16                     |
|                     | 0.28          | $-132.20 \pm 7.14$       | $1.14 \pm 0.04$ | 0.47      | 0.59/7 = 0.08                       |   |                        | 14                     |

TABLE 2—Continued

| Galaxy <sup>a</sup> | $\kappa_\tau$ | $\alpha^b (10^{-6})$ | $\zeta^c$       | $\zeta_o$  | LCM Fit $\frac{\chi^2}{\text{dof}}$ | Other Model $\frac{\chi^2}{\text{dof}}^d$ | Reference <sup>e</sup> | Reference <sup>f</sup> |
|---------------------|---------------|----------------------|-----------------|------------|-------------------------------------|---|------------------------|------------------------|
|                     | 0.29          | $-128.56 \pm 6.96$   | $1.06 \pm 0.03$ | 0.52       | $0.71/7 = 0.10$                     |   |                        | 15                     |
| NGC 4088            | 0.13          | $-59.70 \pm 8.58$    | $1.00 \pm 0.04$ | 1.10       | $30.70/12 = 2.56$                   | $4.41_M$                                  | 13                     | 16                     |
|                     | 0.36          | $-86.94 \pm 12.29$   | $0.99 \pm 0.04$ | 1.04       | $28.71/12 = 2.39$                   |   |                        | 14                     |
|                     | 0.33          | $-81.84 \pm 11.63$   | $0.99 \pm 0.04$ | 1.06       | $29.28/12 = 2.44$                   |   |                        | 15                     |
| NGC 3992            | 0.27          | $-104.95 \pm 9.67$   | $1.00 \pm 0.02$ | 0.93       | $1.81/7 = 0.26$                     | $0.50_M$                                  | 7                      | 16                     |
|                     | 0.33          | $-191.67 \pm 57.59$  | $1.88 \pm 0.07$ | 0.48       | $1.16/3 = 0.39$                     |   |                        | 14                     |
|                     | 0.42          | $-200.39 \pm 60.05$  | $1.30 \pm 0.07$ | 0.66       | $1.09/3 = 0.36$                     |   |                        | 15                     |
| NGC4138             | 0.23          | $-34.20 \pm 6.85$    | $1.00 \pm 0.05$ | 0.88       | $10.65/5 = 2.13$                    | $2.12_M$                                  | 13                     | 16                     |
|                     | 0.64          | $-73.04 \pm 15.01$   | $0.93 \pm 0.05$ | 0.87       | $11.88/5 = 2.38$                    |   |                        | 14                     |
|                     | 0.61          | $-65.70 \pm 13.62$   | $1.00 \pm 0.05$ | 0.91       | $12.36/5 = 2.47$                    |   |                        | 15                     |
| NGC 6946            | 0.09          | $-86.74 \pm 5.20$    | $0.99 \pm 0.02$ | 1.41       | $12.79/18 = 0.71$                   | $3.03_M$                                  | 7                      | 16                     |
|                     | 0.22          | $-103.76 \pm 22.45$  | $0.97 \pm 0.06$ | 1.40       | $7.21/11 = 0.66$                    |   |                        | 14                     |
|                     | 0.21          | $-99.61 \pm 21.76$   | $0.97 \pm 0.06$ | 1.41       | $7.64/11 = 0.69$                    |   |                        | 15                     |
| NGC 6946            | 0.19          | $-111.23 \pm 2.87$   | $0.65 \pm 0.01$ | 1.026      | $157.841/94 = 1.68$                 | $3.67_N$                                  | 4                      | 16                     |
|                     | 0.65          | $-207.90 \pm 5.44$   | $0.45 \pm 0.01$ | 1.246      | $201.33/94 = 2.14$                  |   |                        | 14                     |
|                     | 0.56          | $-208.00 \pm 5.44$   | $0.45 \pm 0.01$ | 1.15       | $201.33/94 = 2.14$                  |   |                        | 15                     |
| NGC3953             | 0.14          | $-150.00 \pm 22.12$  | $1.03 \pm 0.05$ | 0.68       | $3.95/7 = 0.56$                     | $1.35_M$                                  | 7                      | 16                     |
|                     | 0.22          | $-226.06 \pm 33.43$  | $1.80 \pm 0.08$ | 0.38       | $3.94/7 = 0.56$                     |   |                        | 14                     |
|                     | 0.27          | $-213.00 \pm 31.45$  | $1.38 \pm 0.07$ | 0.49       | $3.94/7 = 0.56$                     |   |                        | 15                     |
| NGC 2903            | 0.22          | $-58.90 \pm 1.09$    | $1.00 \pm 0.01$ | 0.92       | $78.31/31 = 2.53$                   | $8.10_M$                                  | 7                      | 16                     |
|                     | 0.49          | $-122.59 \pm 3.57$   | $1.08 \pm 0.01$ | 0.76       | $20.77/23 = 0.90$                   |   |                        | 14                     |
|                     | 0.48          | $-114.76 \pm 3.34$   | $1.04 \pm 0.01$ | 0.80       | $20.66/23 = 0.90$                   |   |                        | 15                     |
| NGC 2903**          | 0.01          | $-311.23 \pm 4.82$   | $1.50 \pm 0.12$ | 0.10       | $2481.72/40 = 62.04$                | $247.18_N$                                | 4                      | 16                     |
|                     | NA            | NA                   | NA              | $10^{-11}$ | NA                                  |   |                        | 14                     |
|                     | NA            | NA                   | NA              | $10^{-12}$ | NA                                  |   |                        | 15                     |
| NGC 2903            | 0.18          | $-75.98 \pm 1.65$    | $1.00 \pm 0.01$ | 1.25       | $54.52/59 = 0.92$                   | $0.53_M$                                  | 5                      | 16                     |
|                     | 0.43          | $-138.60 \pm 4.49$   | $0.99 \pm 0.01$ | 1.13       | $19.59/38 = 0.52$                   |   |                        | 14                     |
|                     | 0.40          | $-129.87 \pm 4.21$   | $0.99 \pm 0.01$ | 1.14       | $20.05/38 = 0.53$                   |   |                        | 15                     |
| NGC5907             | 0.25          | $-82.70 \pm 5.11$    | $1.01 \pm 0.02$ | 0.87       | $3.55/15 = 0.24$                    | $0.48_M$                                  | 13                     | 16                     |
|                     | 0.34          | $-149.26 \pm 18.08$  | $1.86 \pm 0.04$ | 0.45       | $2.45/9 = 0.27$                     |   |                        | 14                     |
|                     | 0.44          | $-151.51 \pm 18.35$  | $1.28 \pm 0.04$ | 0.63       | $2.45/9 = 0.27$                     |   |                        | 15                     |

## 5. Conclusion: Discussion and future work

While the derivation of the LCM is neither fundamental nor Lorentz-invariant, it does provide a working set of assumptions which can be tested against observations. The model is successful in fitting observed rotation curves with the reported luminous matter alone. It is in this sense that the LCM may provide a working constraint to stellar population synthesis models and luminous matter modeling.

Two major goals for future work include extending the LCM formalism to more general geometries of dark matter, and inverting the LCM formalism to predict the preferred luminous matter profile for a specific galaxy given the observed data  $v_{obs}$ .

The first goal, to extend the LCM to a broader category of distance scales and geometries could most easily begin with weak gravitational lensing, (Narayan et al. 1997), as the formalisms are parallel. The LCM symmetry assumptions currently only apply in the plane of the galactic disc, where spherical symmetry can be expected to approximate the functional shape of a disc potential. Furthermore, the general spherical assumptions which are necessary for analytic solution of the wave equation may only generalize to galaxy and globular clusters numerically. Extensions of the LCM formalism even to dynamics above/below the plain of the galactic disc will require intensive numerical modeling of the variations in the potential as well as analysis regarding the appropriate metric. Extension of the LCM to the flat rotation curves of the Milky Way itself will require careful study of how to apply the convolution when the emitter is embedded in within the receiver frame.

The second goal, to use the LCM as a constraint on luminous matter modeling, can be investigated upon identification of a preliminary functional form for the  $\alpha$  parameter as a function of the relative galaxy curvatures  $\kappa_{\tau}$ . Such an inversion protocol would allow the LCM to predict the luminous profile  $M_L$  from the observed data,  $v_{obs}$ .

## 5.1. Acknowledgements

The authors would like to thank V.P. Nair, Ed Bertschinger, Janet Conrad, Marco Inzunza, Peter Fisher, Timothy Boyer, Joel Gersten, and Vassili Papavassiliou. S. Cisneros is supported by the MIT Martin Luther King Jr. Fellowship, while J.A. Formaggio and N.A. Oblath are supported by the United States Department of Energy under Grant No. DE-FG02-06ER- 41420.

TABLE 2—*Continued*

| Galaxy <sup>a</sup> | $\kappa_\tau$ | $\alpha^b (10^{-6})$ | $\zeta^c$       | $\zeta_o$ | LCM Fit $\frac{\chi^2}{\text{dof}}$ | Other Model $\frac{\chi^2}{\text{dof}}^d$ | Reference <sup>e</sup> | Reference <sup>f</sup> |
|---------------------|---------------|----------------------|-----------------|-----------|-------------------------------------|---|------------------------|------------------------|
| NGC 3726            | 0.10          | $-67.30 \pm 9.40$    | $0.99 \pm 0.03$ | 1.35      | $37.43/11 = 3.40$                   | $7.10_M$                                  | 12                     | 16                     |
|                     | 0.29          | $-49.39 \pm 19.08$   | $0.98 \pm 0.04$ | 1.52      | $30.47/8 = 3.81$                    |   |                        | 14                     |
|                     | 0.27          | $-46.70 \pm 18.16$   | $0.98 \pm 0.04$ | 1.53      | $30.59/8 = 3.82$                    |   |                        | 15                     |
| F563-1              | 0.04          | $-47.08 \pm 21.88$   | $0.99 \pm 0.10$ | 4.94      | $0.52/14 = 0.04$                    | $0.05_N$                                  | 9                      | 16                     |
|                     | 0.12          | $-52.98 \pm 24.59$   | $0.97 \pm 0.11$ | 4.91      | $0.51/14 = 0.04$                    |   |                        | 14                     |
|                     | 0.11          | $-51.92 \pm 24.11$   | $0.97 \pm 0.11$ | 4.92      | $0.51/14 = 0.04$                    |   |                        | 15                     |
| NGC925              | 0.03          | $-10.29 \pm 19.20$   | $1.08 \pm 0.08$ | 1.91      | $308.24/45 = 6.85$                  | $3.07_N$                                  | 4                      | 16                     |
|                     | 0.10          | $24.42 \pm 16.98$    | $1.18 \pm 0.06$ | 2.23      | $306.47/45 = 6.81$                  |   |                        | 14                     |
|                     | 0.09          | $18.77 \pm 17.32$    | $1.16 \pm 0.06$ | 2.20      | $307.35/45 = 6.83$                  |   |                        | 15                     |
| NGC 7793            | 0.02          | $-141.10 \pm 7.62$   | $1.04 \pm 0.07$ | 0.73      | $265.74/48 = 5.54$                  | $4.11_M$                                  | 5                      | 16                     |
|                     | 0.02          | $-269.99 \pm 12.34$  | $1.16 \pm 0.17$ | 0.27      | $324.48/47 = 6.90$                  |   |                        | 14                     |
|                     | 0.05          | $-144.90 \pm 7.91$   | $1.05 \pm 0.07$ | 0.71      | $273.82/48 = 5.70$                  |   |                        | 15                     |

14. Sofue 1981, 15. Klypin 2002, model A (*no* exchange of angular momentum), 16. Klypin 2002, model B

<sup>a</sup>Results marked with \*\* indicate a fit that did not converge.

<sup>b,c</sup>Uncertainties are statistical only.

<sup>d</sup>N=NFW; M=MOND; blank indicates model independent.

<sup>e</sup>Emitter-galaxy references: as in Table 1

<sup>f</sup>MW References: 14. Klypin et al. (2002) model A (*no* exchange of angular momentum), 15. Klypin et al. (2002) model B (*with* exchange of angular momentum), 16. Sofue & Kato (1981).

## REFERENCES

- Aalseth, C. et al. 2013, PhysRev, D88, 012002
- Agnese, R. et al. 2013, PhysRevLett
- Angle, J. et al. 2008, PhysRevLett, 100, 021303
- Asaoka, I. 1989, PASJ, 41, 763
- Battaglia, G., Fraternali, F., Oosterloo, T., , & Sancisi, R. 2006, A& A, 447, 49
- Bernabei, R. et al. 2010, EurPhysJ, C67, 39
- Binney, J. & Tremaine, S. 2008, *Galactic Dynamics*, Princeton University Press: Princeton, NJ, 2nd edn.
- Born, M. & Wolf, E. 1999, *Principles of Optics*, Cambridge University Press, 9th edn.
- Bosma, A. 1978, *The distribution and kinematics of neutral hydrogen in spiral galaxies of various morphological types*, Ph.D. thesis, University of Groningen, Rijksuniversiteit Groningen
- Bottema, R. & Pestana, J. 2002, A&A, 393, 453
- Brun, R. & Rademakers, F. 1997, Nucl Inst & Meth in Phys Res A, 389, 81
- Carignan, C. & Chemin, L. 2006, ApJ, 641, L109
- Chandrasekhar, S. 1983, *The Mathematical Theory of Black Holes*, Oxford University Press, New York, NY
- Chatterjee, T. 1987, Ap&SS, 139, 243
- Cisneros, S., Goedecke, G., Beetle, C., & Engelhardt, M. 2012, “On the Doppler effect for light from orbiting sources in Kerr-type metrics”, ArXiv:1203.2502
- Conroy, C., Gunn, J., & White, M. 2009, ApJ, 699, 486
- Corbelli, E. 2003, MNRAS, 342, 199
- de Blok, W., Walter, F., , & Brinks, E. 2008, AJ, 136, 2648
- Einstein, A., Lorentz, H.A., Minkowski, H., & Weyl, H. 1923, *The Principle of Relativity*, Dover Publications
- Fowles, G. & Cassidy, G. 2005, *Analytical Mechanics*, Thomson Brooks & Cole: Belmont, CA, USA, 7th edn.
- Fraternali, F., Sancisi, R., , & Kamphuis, P. 2011, A&A, <http://arxiv.org/abs/1105.3867>
- Gentile, G., Farnaey, B., & de Blok, W. 2011, A&A, 527, A76
- Gentile, G., Jozsa, G., Serra, P., Heald, G., de Blok, W., Fraternali, F., Patterson, M., Walterbos, R., & Oosterloo, T. in press, A& A, arXiv:1304.4232
- Gianfranco, B., Hooper, D., & Silk, J. 2005, Physics Reports, 405, 279
- Hartle, J. 2003, *Gravity*, Addison-Wesley
- Jackson, J. 1999, *Classical Electrodynamics*, John Wiley & Sons, Inc., New Jersey, USA, 3rd edn.
- Klypin, A., Zhao, H., & Somerville, R. 2002, ApJ, 573, 597
- Milgrom, M. 1983, ApJ, 270, 371
- Misner, C., Thorne, K., & Wheeler, J. 1970, *Gravitation*, W.H. Freeman and Company, New York, NY, USA
- Narayan, R., , & Bartelman, M. 1997, *Formation of Structure in the Universe: Lectures on Gravitational Lensing*, A Dekel, JP Ostriker
- Navarro, J. 1998, “The Cosmological Significance of Disk Galaxy Rotation Curves”, Astroph/9807084
- Navarro, J., Frenk, C., & White, S. 1997, ApJ, 462, 563
- O’Neill, B. 1995, *The Geometry of Kerr Black Holes*, A. K. Peters, Wellesley, MA, USA
- Persic, M., Salucci, P., , & Stel, F. 1996, MNRAS, 281, 27
- Persic, M. & Salucci, P. 1997, in “Dark and visible matter in Galaxies”, ASP Conference Series 117, 1
- Rubin, V. & Ford, W. 1975, in “Conference Proceedings AAS”, AAS

- Rubin, V., Ford, W., & Thonnard, N. 1980, *ApJ*, 238, 471
- Sanders, R. 1996, *ApJ*, 473, 117
- Sanders, R. & McGaugh, S. 2002, *ARA&A*, 40, 263
- Sanders, R. & Verheijen, M. 1998, *ApJ*, 503, 97
- Seigar, M. 2011, *ISRN A&A*, arXiv:1103.3200v1
- Smith, R. 1995, *Observational Astrophysics*, Cambridge University Press, Cambridge, UK
- Sofue, Y. & Kato, T. 1981, *Publ Astron Soc Japan:Astronomical Society of Japan*, 33, 449
- van den Bergh, S. 1997, *ApJ*, 113, 2054
- Wald, R. 1984, *General Relativity*, University of Chicago Press, Chicago, IL, USA
- Zwicky, F. 1937, *ApJ*, 86, 217